Supplementary Information (SI) for ChemComm.

Contents

S1. General methods

Synthesis: All the synthetic manipulations were performed under a dry an argon atmosphere using standard Schlenk techniques. Unless otherwise noted, materials obtained from commercial suppliers were used without further purification. Column chromatography was performed using Wako Silica-gel 70 PF254 or Kanto Silica Gel 60 (spherical, particle size 100-210 μm).

***^{1}H and ^{13}C-NMR measurements*:** ^{1}H-, ^{13}C-, spectra were recorded with a Bruker AVANCE III (^{1}H-NMR 400 MHz, ^{13}C-NMR 100 MHz). Variable temperature (VT)-NMR measurements were recorded with a JEOL ECS-400 (^{1}H-NMR 400 MHz). ^{1}H-NMR spectra are reported as follows: chemical shift in ppm relative to the chemical shift of CD_2Cl_2 at 5.32 ppm, integration, multiplicities (*s* = singlet, *d* = doublet, *t* = triplet, *dd* = double doublet, *m* = multiplet), and coupling constants (*Hz*). ^{13}C-NMR spectra reported in ppm relative to the central line of quintet for CD_2Cl_2 at 53.84 ppm.

Cyclic voltammetry: Electrochemical measurements were performed under dry argon atmosphere using a BAS Electrochemical Analyzer Model 1210C, a glassy carbon working electrode (diameter: 3 mm), a Pt wire counter electrode, and an Ag wire/$AgNO_3$ in MeCN reference electrode.

***Mass spectrometry*:** High-resolution mass spectra (HRMS) were recorded on a Bruker micrOTOF mass spectrometer (ionization mode: APCI or ESI). Tuning Mix (Agilent Technologies, Inc.) or sodium formate in MeOH was used as an external standard.

Variable temperature (VT) ESR measurements: ESR spectra were recorded on an X-band ESR spectrometer (JES-FA200; JEOL). The *g*-factor and ESR signal intensity were calibrated based on Mn^{2+} marker signal.

***Ultraviolet-visible-near infrared (UV-vis-NIR)* spectroscopy:** UV-vis-NIR spectra were recorded on a Shimadzu UV-3101PC spectrometer.

Single crystal X-ray (scXRD) diffraction: scXRD measurements were carried out on a Rigaku MicroMax-007HF diffractometer equipped with a VariMax light source (Mo Kα, λ = 0.71073 Å).

S2. Synthesis

Br$_2$DBAB[S1] and tris(4-bromophenyl)ammoniumyl hexafluoroantimonate[S2] were synthesized following the reported procedures.

Synthesis of Dpa$_2$DBAB

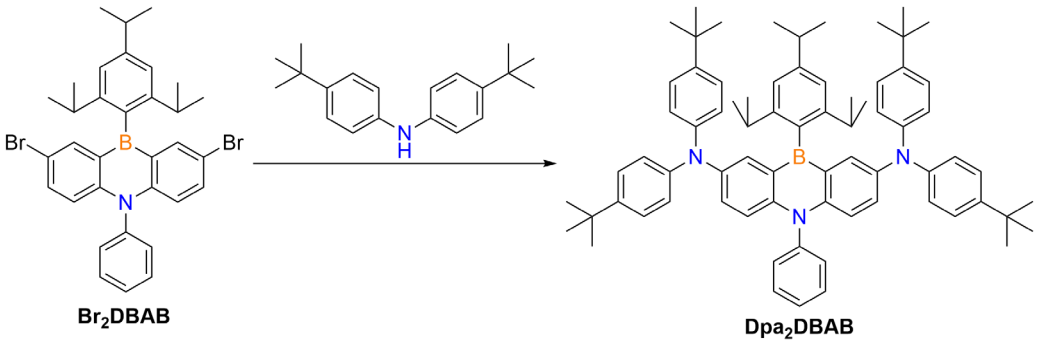

Scheme S1. Synthesis of **Dpa$_2$DBAB**

A toluene (50 mL) solution of **Br$_2$DBAB** (1.00 g, 1.63 mmol), bis(4-*tert*-butylphenyl)amine (0.96 g, 3.41 mmol), $Pd(OAc)_2$ (0.04 g, 0.16 mmol), [*t*Bu$_3$PH]BF_4 (0.18 g, 0.33 mmol) and *t*BuONa (0.94 g, 9.75 mmol) was stirred at 110 °C for 48 h. The reaction was quenched with aq. NH_4Cl and extracted with ethyl acetate. The organic layer was dried over Na_2SO_4 and concentrated. The mixture was purified by column chromatography (SiO_2, hexane to hexane/dichloromethane 10:1 to 1:1 *v*/*v*) to afford **Dpa$_2$DBAB** (0.40 g, 0.39 mmol, 24%) as a light yellow solid.
Note: **Dpa$_2$DBAB** is light and air sensitive. The color gradually changed from light yellow to light green under air. Therefore, **Dpa$_2$DBAB** was kept under an argon atmosphere in the dark.

^{1}H-NMR (400 MHz, CD_2Cl_2): δ = 7.64 (*t*, *J* = 7.6 Hz, 2H), 7.55 (*t*, *J* = 7.6 Hz, 2H), 7.41−7.38 (*m*, 4H), 7.17 (*dd*, *J* = 4.7, 2.6 Hz, 2H), 7.05 (*d*, *J* = 9.2 Hz, 8H), 6.80 (*s*, 2H), 6.75 (*d*, *J* = 8.8 Hz, 8H), 6.70 (*d*, *J* = 9.2 Hz, 2H), 2.79−2.73 (*m*, 1H), 2.34−2.27 (*m*, 2H), 1.16−1.14 (*m*, 42H), 0.79 (*d*, *J* = 6.8 Hz, 12H). (Figure S17)

^{13}C-NMR (100 MHz, CD_2Cl_2): δ = 150.6, 148.2, 146.0, 144.7, 143.5, 142.3, 140.0, 134.3, 132.6, 131.3, 130.6, 129.5, 126.2, 122.2, 120.0, 118.7, 35.4, 34.5(2), 34.5(4), 24.5, 24.2. (Two signals corresponding to B-C carbon could not be observed, Figure S18)

HRMS (APCI, Positive) calcd. for $C_{73}H_{86}BN_3$ $[M+nH]^+$: 1016.6999. Found: 1016.6848. (Figure S19)

Synthesis of [Dpa$_2$DBAB](SbF$_6$)$_2$

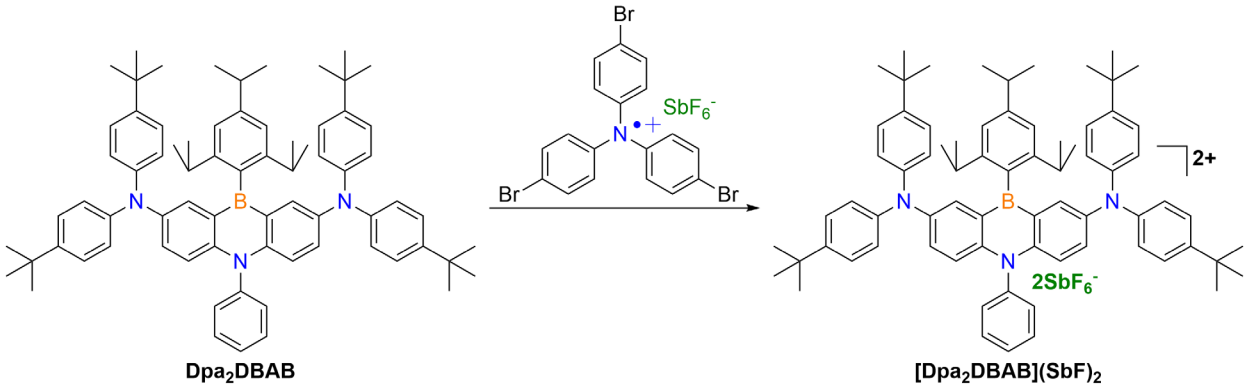

Scheme S2. Synthesis of [**Dpa$_2$DBAB**](**SbF$_6$**)$_2$

A dichloromethane (15 mL) solution of **Dpa$_2$DBAB** (50.0 mg, 0.05 mmol) and **MB** (77.7 mg, 0.11 mmol) was stirred at 20℃ for 2 h in the dark. To the mixture, diethyl ether was added slowly and cooled to 0 °C slowly. The precipitated crystals were further washed by diethyl ether to afford **[Dpa$_2$DBAB](SbF$_6$)$_2$** (33.4 mg, 0.02 mmol, 45%) as dark violet crystals.

HRMS (ESI, Positive): Calcd. for $C_{73}H_{86}BN_3SbF_6$ $[M]^+$: 1252.5852. Found: 1252.6041. (Figure S20)

Anal.: Calcd. For $C_{73}H_{86}BN_3Sb_2F_{12} + CH_2Cl_2 + C_4H_{10}O$: C, 56.89; H, 6.00; N, 2.55%. Found: C, 56.55; H, 6.01; N, 2.62%.

S3. Supplementary Details of Cyclic voltammetry Measurements and Analysis

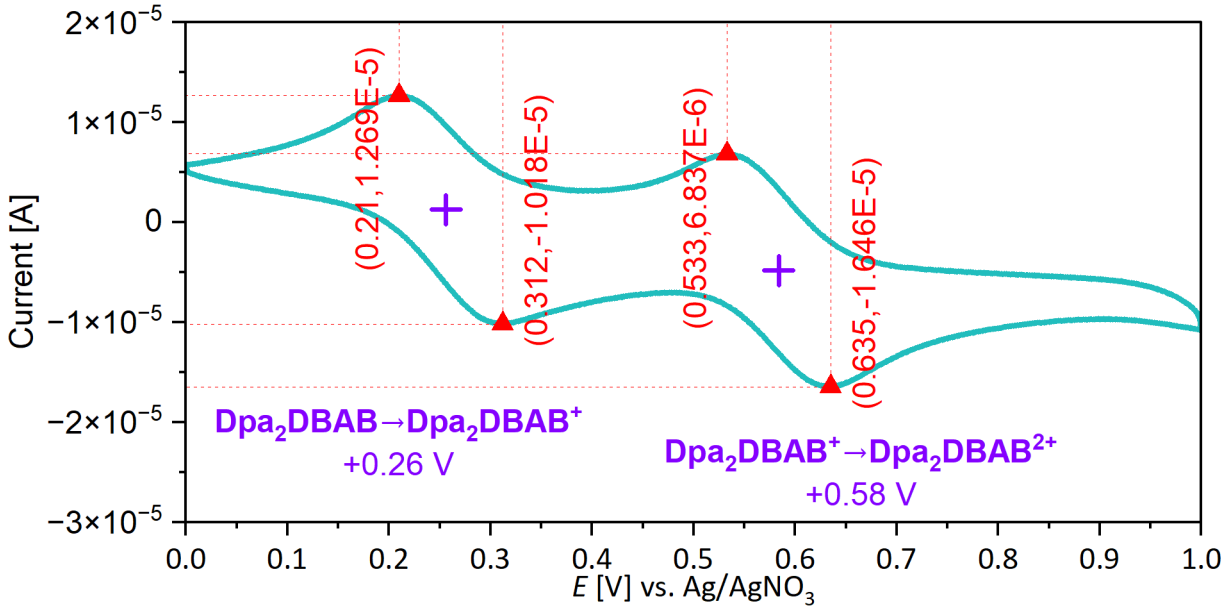

Figure S1. Oxidation and reduction peaks, as well as the estimated oxidation potentials of **Dpa$_2$DBAB**.

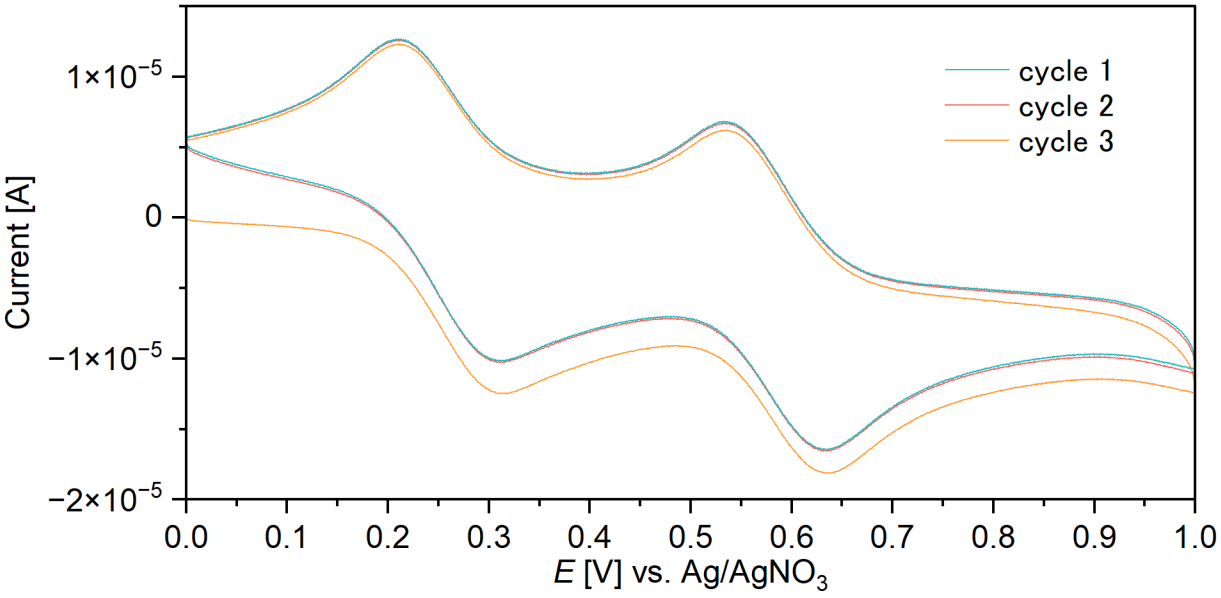

Figure S2. Repeated cyclic voltammograms (3 cycles) of **Dpa$_2$DBAB**.

S4. Single crystal X-ray Diffraction Measurements and Analysis

Single crystal X-ray diffraction (scXRD) measurements were carried out on a Rigaku MicroMax-007HF diffractometer equipped with a VariMax light source (Mo Kα, λ = 0.71073 Å). The crystals were kept at –100 °C while the data collection. The collected data were processed using the CrysAlisPro (ver. 1.171.41.117a) program package (Rigaku Oxford Diffraction, 2021). Using Olex2,[S3] the structures were solved with the SHELXT and refined with the SHELXL program packages.[S4] The full-matrix least-squares refinements were performed on F_2. All non-hydrogen atoms were refined anisotropically. Hydrogen atoms were refined using the riding model. Two counter SbF_6^- anions and one Et_2O molecule were found per one **Dpa$_2$DBAB^{2+}** moiety (Figure S3, Figure S4). The two SbF_6^- counter anions were disordered over two sites, with the occupancy ratios of 0.294:0.706 and 546:454, respectively. The SIMU and RIGU restraints were included for the anisotropic displacement parameters of these disordered counter anions. CCDC 2387211 (**[Dpa$_2$DBAB](SbF$_6$)$_2$**) contains the additional crystallographic data.[S5]

Table 1. Crystallographic data for **[Dpa$_2$DBAB](SbF$_6$)$_2$**

[Dpa$_2$DBAB](SbF$_6$)$_2$	
Empirical formula	$C_{77}H_{96}BF_{12}N_3OSb_2$
Formula weight	1561.87
Temperature/K	173.15
Crystal system	triclinic
Space group	*P*-1
a/Å	15.2096(4)
b/Å	16.6088(6)
c/Å	17.4936(7)
α/°	63.221(4)
β/°	81.517(3)
γ/°	89.492(3)
Volume/Å^3	3893.7(3)
Z	2
ρ_{calcd}/g cm^{-3}	1.332
μ/mm^{-1}	0.765
F(000)	1604.0
Crystal size/mm^3	0.113 × 0.095 × 0.055
Radiation	Mo *K*α (λ = 0.71073)
2***Θ*** range for data collection/°	5.576 to 59.768
Index ranges	-21 ≤ h ≤ 20, -23 ≤ k ≤ 23, -24 ≤ l ≤ 23
Reflections collected	61213
Independent reflections	20095 [R_{int} = 0.0477, R_{sigma} = 0.0738]
Data/restraints/parameters	20095/924/1013
Goodness-of-fit on F^2	1.016
Final ***R*** indexes [***I***>=2***σ*** (***I***)]	R_1 = 0.0591, wR_2 = 0.1270
Final ***R*** indexes [all data]	R_1 = 0.1075, wR_2 = 0.1437
Largest diff. peak and hole / e Å^{-3}	0.90/-0.68

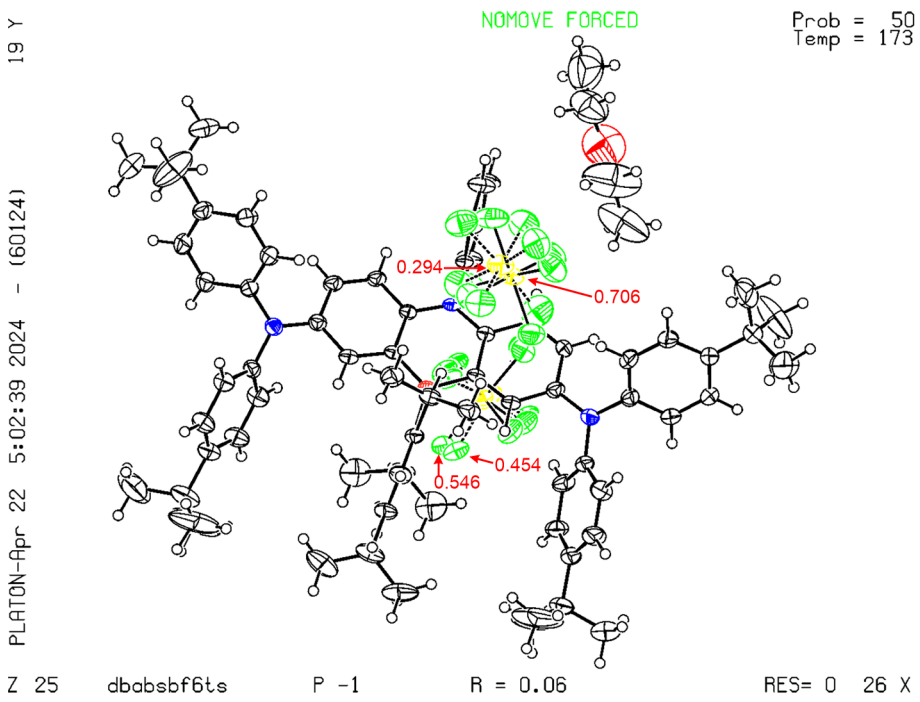

Figure S3. Thermal ellipsoid plots of **[Dpa$_2$DBAB](SbF$_6$)$_2$** with one Et_2O molecule and disordered counter **SbF$_6^-$** anions.

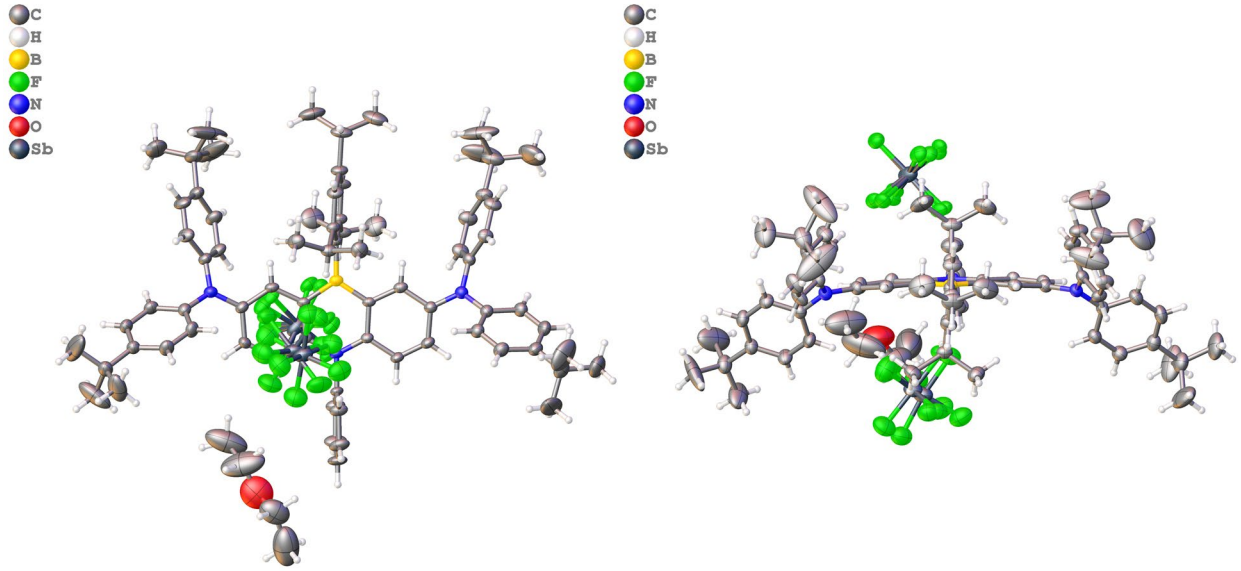

Figure S4. Top view (left) and side view (right) of the scXRD detected molecular structures of **[Dpa$_2$DBAB](SbF$_6$)$_2$**.

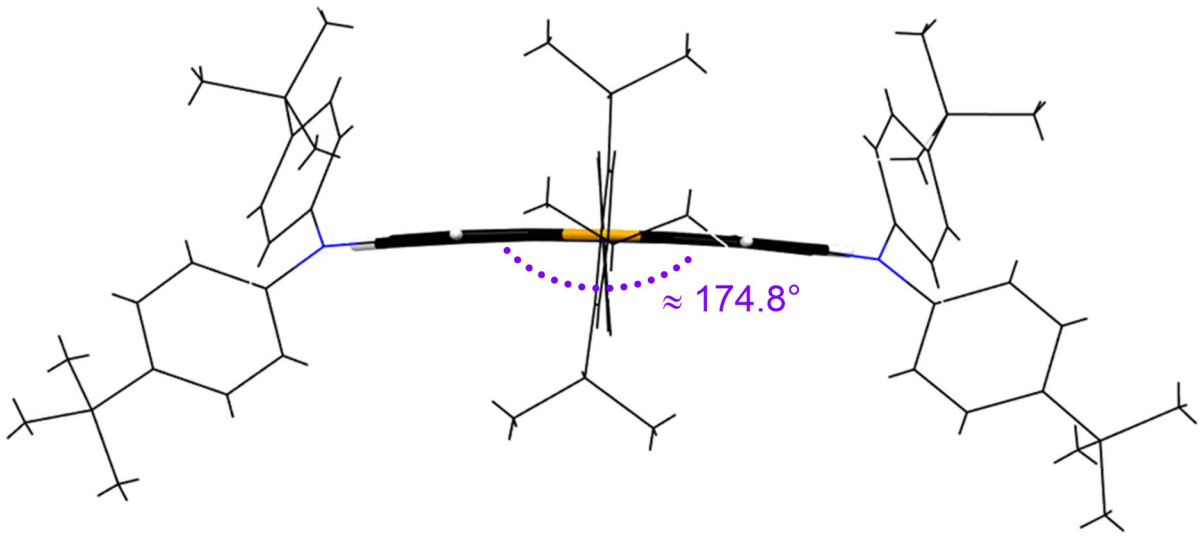

Figure S5. Side view of **[Dpa$_2$DBAB](SbF$_6$)$_2$** showing the curvature of the dibenzo-1,4-azaborine moiety.

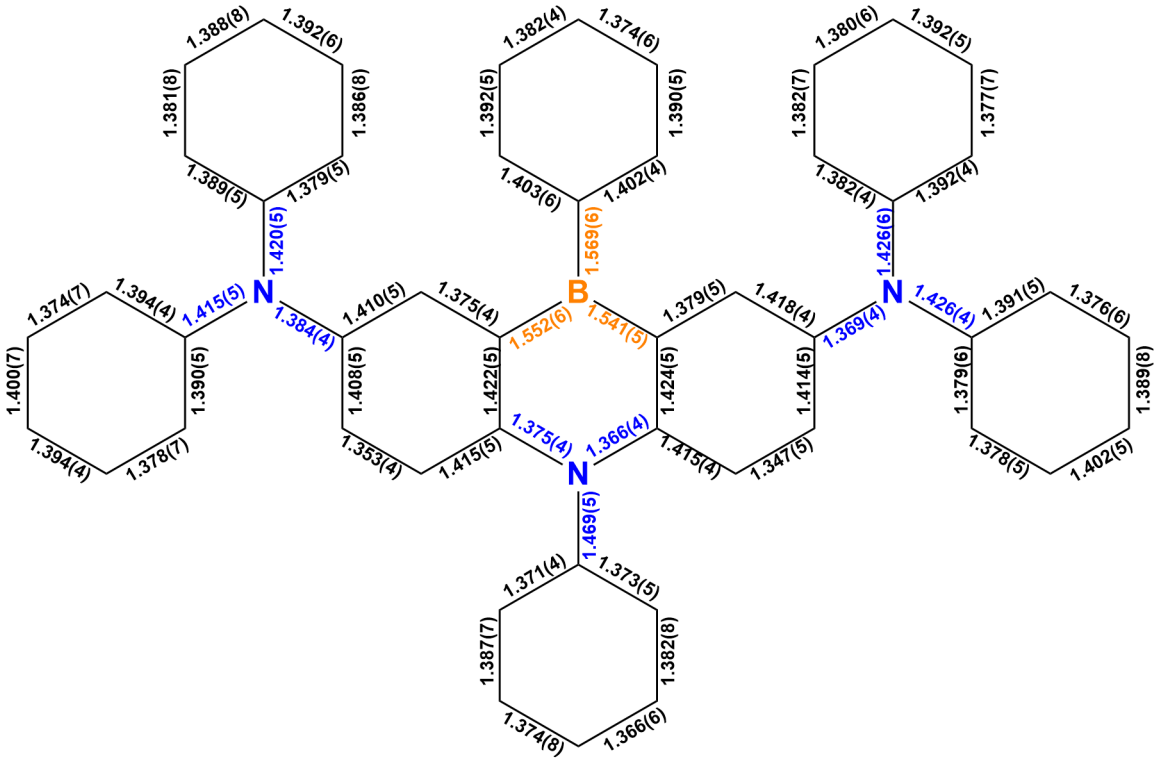

Figure S6. scXRD-determined bond lengths of the conjugated system of **Dpa$_2$DBAB^{2+}**.

S5. Electron Spin Resonance (ESR) Measurements

Powder of **[Dpa$_2$DBAB](SbF$_6$)$_2$** was used for the VT-ESR measurements and the VT-ESR data was fitted by modified Bleaney-Bowers equation. Here, we describe the approach to the singlet-triplet energy gap $\Delta E_{S\text{-}T}$.

As there was no significant change in the linewidth of the signals, the ESR signal intensity of powder **[Dpa$_2$DBAB](SbF$_6$)$_2$** normalized by Mn^{2+} marker obeys:

$$I_{Singal}/I_{Mn} \propto \chi \qquad [Eq.S1]$$

where I_{singal} is the double integral of the **[Dpa$_2$DBAB](SbF$_6$)$_2$** ESR spectral, I_{Mn} is the double integral of the Mn^{2+} mark signal, χ is the magnetic susceptibility.

By letting χ (arb. unit) be I_{singal}/I_{Mn}, the χ (arb. unit) is expected to follow the Bleaney-Bowers equation below:

$$\chi = \frac{1}{T}\frac{A}{3 + \exp\left(-\frac{\Delta E_{S-T}}{k_B T}\right)} \qquad [Eq.S2]$$

where A is a constant, k_B is Boltzmann constant.

In this study, to correspond the contribution of paramagnetic impurity, the equation was modified with an offset obeying the Curie's law:

$$\chi = \frac{B}{T} + \frac{1}{T}\frac{A}{3 + \exp\left(-\frac{\Delta E_{S-T}}{k_B T}\right)} \qquad [Eq.S3]$$

where B is a constant.

Based on equation S3, a fitting on the χT *vs.* T plot of **[Dpa$_2$DBAB](SbF$_6$)$_2$** was carried out via the following equation:

$$\chi T = B + \frac{A}{3 + \exp\left(-\frac{C}{T}\right)} \qquad [Eq.S4]$$

where A and B are constant, C could be expressed by the following equation:

$$C = \frac{\Delta E_{S-T}}{k_B} = \frac{2J}{k_B} \qquad [Eq.S5]$$

The fitting gave a C in −674 K, and the $\Delta E_{S\text{-}T}$ was calculated out in −1.34 kcal mol^{-1}.

Details of earned curve and the values of each parameter were shown below with error (Figure S7).

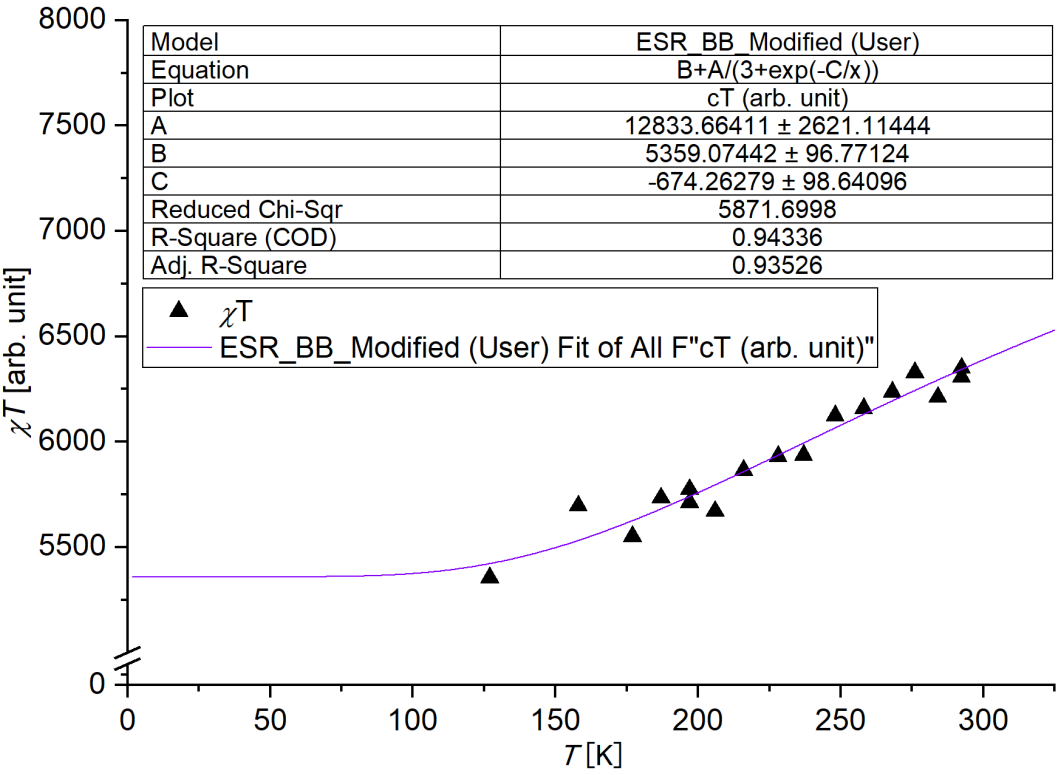

Figure S7. χT-T plot for the dication with the fitting curve obtained using the modified Bleaney-Bowers equation. The obtained values of parameters with error bar were also shown.

Table S2. Used date for the χT-T plot. (χ [arb. unit] = I_{signal}/I_{Mn})

T	$1/T$	I_{Mn}	I_{singal}	I_{signal}/I_{Mn}	χT [arb. unit]
292.3	0.003421	1572	33918	21.58	6307
197	0.005076	1391	40764	29.31	5773
177	0.00565	1361	42684	31.36	5551
127	0.007874	1130	47646	42.16	5355
158	0.006329	971	35007	36.05	5696
187	0.005348	822	25206	30.66	5734
197	0.005076	877	25428	28.99	5712
206	0.004854	896	24660	27.52	5670
216	0.00463	901	24461	27.15	5864
228	0.004386	979	25463	26.01	5930
237	0.004219	1043	26126	25.05	5937
248	0.004032	1082	26719	24.69	6124
258	0.003876	1170	27930	23.87	6159
268	0.003731	1272	29599	23.27	6236
276	0.003623	1425	32672	22.93	6328
284	0.003521	1552	33947	21.87	6212
292.3	0.003421	1518	32980	21.73	6350

S6. Theoretical Calculations

All theoretical calculations of **[Dpa$_2$DBAB](SbF$_6$)$_2$** were performed with Gaussian 16 (Revision C.02) program package.[S6] The method (U)B3LYP density functional and the 6-311G(d) basis sets were employed for geometry optimizations. All optimized structures were verified by frequency analysis that corresponded to the equilibrium structures.

Supplemental details of optimizations

Table S3. Summary of methods used for optimizations[a]

Compound		Method				Additional Conditions
Dpa$_2$DBAB	-	DFT	6-311G(d)	Default Spin	B3LYP	-
Dpa$_2$DBAB^{1+}	-	DFT	6-311G(d)	Unrestricted	B3LYP	-
Dpa$_2$DBAB^{2+}	**CS**	DFT	6-311G(d)	Default Spin	B3LYP	-
	OS	DFT	6-311G(d)	Unrestricted	B3LYP	guess=mix,read[b]
	T	DFT	6-311G(d)	Unrestricted	B3LYP	-
1^{2+}	**CS**	DFT	6-311G(d)	Default Spin	B3LYP	-
	OS	DFT	6-311G(d)	Unrestricted	B3LYP	guess=mix
	T	DFT	6-311G(d)	Unrestricted	B3LYP	-
2^{2+}	**CS**	DFT	6-311G(d)	Default Spin	B3LYP	-
	OS	DFT	6-311G(d)	Unrestricted	B3LYP	guess=mix
	T	DFT	6-311G(d)	Unrestricted	B3LYP	-

[a] CS = closed-shell singlet, OS = open-shell singlet, T = triplet. [b] Molecular orbitals of optimized **Dpa$_2$DBAB^{2+}** (**T**) were used as initial conditions.

Calculations on the harmonic oscillator model of aromaticity

The harmonic oscillator model of aromaticity (HOMA) was calculated with the experimental an optimized bond lengths (R_i) of **Dpa$_2$DBAB^{2+}** according to the following equation:[12S7]

$$HOMA = 1 - \frac{\alpha}{n}\sum_{i}^{n}\left(R_{opt} - R_i\right)^2 \qquad [Eq.S6]$$

with an empirical normalization constant α = 98.89, which gives HOMA = 0 for a model nonaromatic system and HOMA = 1 for a benzene-approximated system where all bonds are equal to the optimal bond length (R_{opt} = 1.397 Å).

Here, the R_{opt} can be represented using the reference values of CC bond lengths in ethane (R_{C-C} = 1.524 Å) and ethene ($R_{C=C}$ = 1.334 Å) according to the following equation:[S7]

$$R_{opt} = \frac{(R_{C-C} + 2R_{C=C})}{3} = 1.397 \text{ Å} \qquad [Eq.S7]$$

where the relation between force constants for single and double bonds are assumed to be 1:2.[S7]

Calculations on the diradical characters and singlet-triplet energy gap

The diradical character y was calculated from the occupation number of the highest occupied natural orbital (n_{HONO}) and of the lowest unoccupied natural orbital (n_{LUNO}) according to the following equation:[14S8]

$$y = 1 - \frac{2T}{1 + T^2} \qquad [Eq.S8]$$

where T is the orbital overlap between the corresponding orbital pairs, which can be represented using the n_{HONO} and n_{LUNO}:[14S8]

$$T = \frac{n_{HONO} - n_{LUNO}}{2} \qquad [Eq.S9]$$

The singlet-triplet energy gap ($\Delta E_{S\text{-}T}$) was calculated with the Yamaguchi spin decontamination correction according to the following equation:[21S9]

$$\Delta E_{S-T} = \frac{(E_{OS} - E_T) < S^2 >_T}{< S^2 >_T - < S^2 >_{OS}} \qquad [Eq.S10]$$

where E_T and E_{OS} represent the summary of the electronic and zero-point energies calculated at triplet (**T**) and open-shell state (**OS**). $\langle S^2\rangle_T$ and $\langle S^2\rangle_{OS}$ correspond to their respective spin contamination.

Supplemental date on comparisons of structures and diradical characters

Table S4. Summary of optimized structures of **Dpa$_2$DBAB^{2+}**.

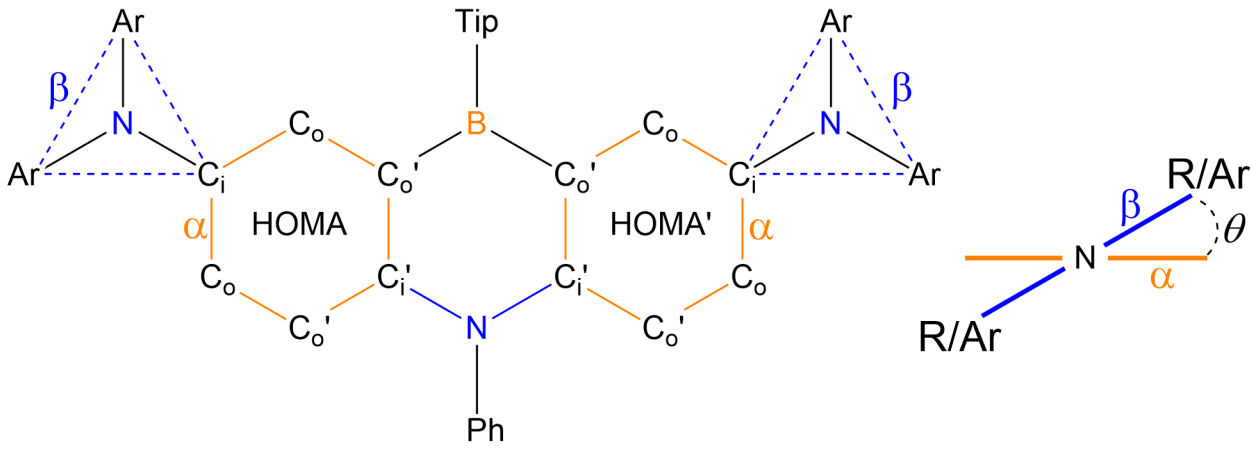

Structure	*avg* C_i-N [Å]	*avg* C_o-C_o [Å]	*avg* θ [deg]	*avg* HOMA[e]
scXRD	1.374	1.364	33.3[c]	0.932
CS[a,b]	1.383	1.380	30.9[d]	0.945
OS[a,b]	1.399	1.387	38.3[d]	0.966
T[a,b]	1.404	1.389	41.1[d]	0.968

[a] Optimized at (U)B3LYP/6-311G(d) level. [b] **CS** = closed-shell singlet, **OS** = open-shell singlet, **T** = triplet. [c] Estimated from the scXRD-detected structure with Olex2.[S3] [d] Estimated using the optimized structures with Mercury 4.0 (ver 4.2.0).[S10] [e] The harmonic oscillator model of aromaticity.[S7]

Table S5. Summary of calculated energy gaps and diradical characters of **Dpa$_2$DBAB^{2+}**.

Structure	E_X [Eh][d,e]	$\Delta E_{X\text{-}OS}$ [kcal mol^{-1}][e]	y[f]	n_{HONO}	n_{LUNO}	s^2
scXRD	-	-	0.324[g]	1.38953[g]	0.61047[g]	
CS[a,b]	−3021.480598[b]	+5.87	0.326[g]	1.38774[g]	0.61226[g]	0.8733
OS[a,c]	−3021.489955[c]	0	0.478[c]	1.28198[c]	0.71802[c]	0.9462
T[a,c]	−3021.488694[c]	+1.48	-	-	-	

[a] **CS** = closed-shell singlet, **OS** = open-shell singlet, **T** = triplet. [b] Optimized/calculated at B3LYP/6-311G(d) level. [c] Optimized/calculated at UB3LYP/6-311G(d) level. [d] The summary of the electronic and zero-point energies. [e] **X** = **CS**, **OS**, **T**. [f] Diradical character. [g] Calculated on the scXRD/**CS** geometry at UB3LYP/6-311G(d) level.

Table S6. Selected calculated data of reference compounds dication $\mathbf{1}^{2+}$ and $\mathbf{2}^{2+}$ with reported data

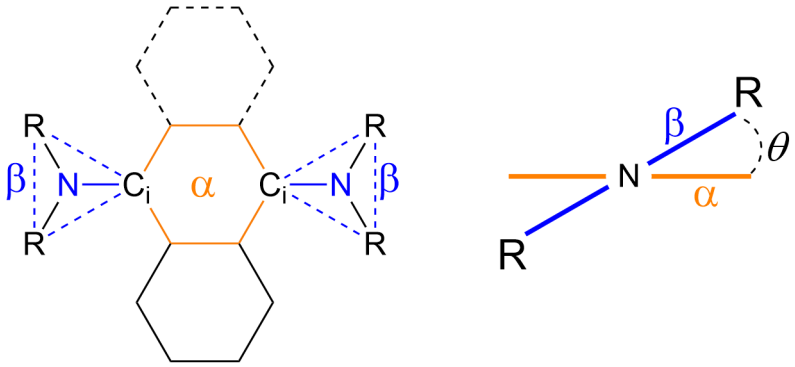

			avg C_i-N [Å]	*avg*θ [deg]	$\Delta Ex\text{-}os$ [kcal mol^{-1}][e]	y^f	n_{HONO}	n_{LUNO}
$\mathbf{1}^{2+}$	**CS**[a,b]	This work	1.385	41.1[d]	1.96	-	-	-
	OS[a,b]		1.420	51.1[d]	0	0.251[b]	1.45007	0.54993
	T[a,b]		1.440	60.7[d]	2.78	-	-	-
	scXRD	Ref. [S11]	1.354 (3)	33.0	-	-	-	-
	CS[a,c]		1.380	-	1.82	-	-	-
	OS[a,c]		1.400	-	0	0.18[g]	-	-
	T[a,c]		1.439	-	3.26	-	-	-
$\mathbf{2}^{2+}$	CS[a,c]	This work	1.399	54.85[d]	3.71	-	-	-
	OS[a,c]		1.439	68.67[d]	0	0.516[b]	1.25831	0.74169
	T[a,c]		1.450	72.86[d]	1.42	-	-	-
	scXRD	Ref. [S11]	1.405(4)	56.2	-	-	-	-
	CS[a,c]		1.394	-	3.26	-	-	-
	OS[a,c]		1.437	-	0	0.63[g]	-	-
	T[a,c]		1.445	-	1.47	-	-	-

[a] **CS** = closed-shell singlet, **OS** = open-shell singlet, **T** = triplet. [b] Optimized at (U)B3LYP/6-311G(d) level. [c] Optimized at (U)B3LYP/6-31G(d) level. [d] Estimated using the DFT-optimized structures with Mercury 4.0 (ver 4.2.0).[S10] [e] **X** = **CS**, **OS**, **T**. [f] Diradical character. [g] Calculated at UBHandHLYP/6-31G(d) level.[S11]

Table S7. Summary of optimized structures of **Dpa$_2$DDAD^{2+}** (Ar = 4-*tert*-butylphenyl).

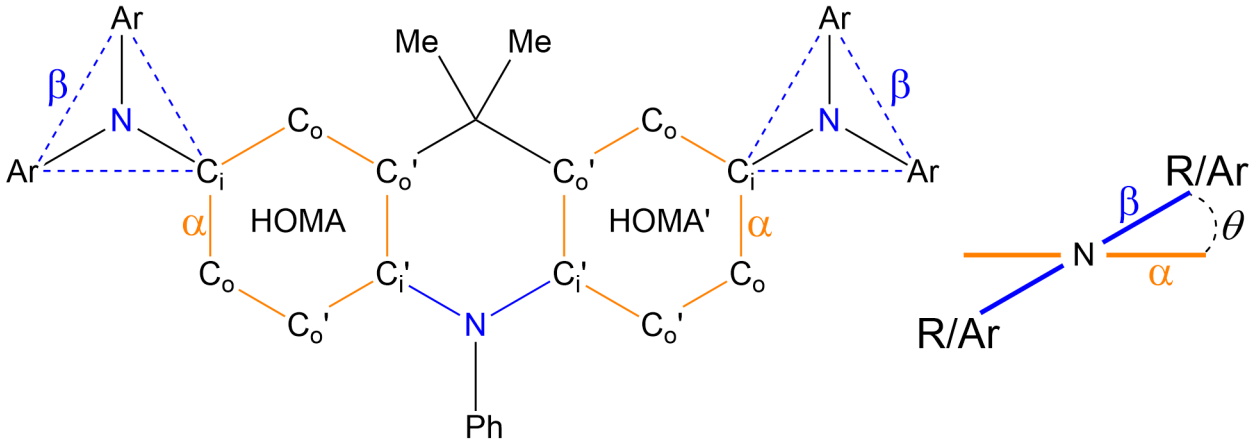

Structure	*avg* C_i-N [Å]	*avg* C_o-C_o [Å]	*avg* θ [deg]	*avg* HOMA[e]
CS[a,b]	1.379	1.372	26.4[d]	0.941
OS[a,b]	1.376	1.372	26.4[d]	0.941
T[a,b]	1.400	1.382	36.7[d]	0.980

[a] Optimized at (U)B3LYP/6-311G(d) level. [b] **CS** = closed-shell singlet, **OS** = open-shell singlet, **T** = triplet. [c] Estimated from the scXRD-detected structure with Olex$_2$.[S3] [d] Estimated using the optimized structures with Mercury 4.0 (ver 4.2.0).[S10] [e] The harmonic oscillator model of aromaticity.[S7]

Table S8. Summary of calculated energy gaps and diradical characters of **Dpa$_2$DDAD^{2+}**.

Structure	E_X [Eh][d,e]	$\Delta E_{X\text{-}OS}$ [kcal mol^{-1}][e]	y[f]	n_{HONO}	n_{LUNO}
CS[a,b]	–2529.226087[b]	0	-	-	-
OS[a,c]	–2529.225087[c]	0	0	-	-
T[a,c]	–2529.227747[c]	+1.04	-	-	-

[a] **CS** = closed-shell singlet, **OS** = open-shell singlet, **T** = triplet. [b] Optimized/calculated at B3LYP/6-311G(d) level. [c] Optimized/calculated at UB3LYP/6-311G(d) level. [d] The summary of the electronic and zero-point energies. [e] **X** = **CS**, **OS**, **T**. [f] Diradical character. [g] Calculated on the scXRD/**CS** geometry at UB3LYP/6-311G(d) level.

Supplemental details of TD-DFT calculations

Based on the optimized ground state structure of **Dpa$_2$DBAB^{2+}** at **CS**, **OS** and **T** sates, respectively, twenty excited singlet states and twenty excited triplet states were calculated. Additionally, twenty excited singlet states and twenty excited triplet states of **Dpa$_2$DBAB** as well as twenty excited doublet states of **Dpa2DBAB^{+}** were calculated based on the optimized structure at the same level. Simulated absorption spectra and selected MOs relevant for calculated excited states of **Dpa$_2$DBAB**, **Dpa$_2$DBAB^{1+}** and **Dpa$_2$DBAB^{2+}** are shown below

Table S9. Summary of methods used for TD-DFT calculations[a,b]

Compound		Method				Additional Conditions
Dpa$_2$DBAB		DFT	6-311G(d)	Default Spin	B3LYP	-
Dpa$_2$DBAB^{1+}		DFT	6-311G(d)	Unrestricted	B3LYP	-
Dpa$_2$DBAB^{2+}	**CS**	DFT	6-311G(d)	Default Spin	B3LYP	-
	OS	DFT	6-311G(d)	Unrestricted	B3LYP	guess=mix
	T	DFT	6-311G(d)	Unrestricted	B3LYP	-

[a] **CS** = closed-shell singlet, **OS** = open-shell singlet, **T** = triplet. [b] Calculated on geometries optimized at (U)B3LYP/6-311G(d) level.

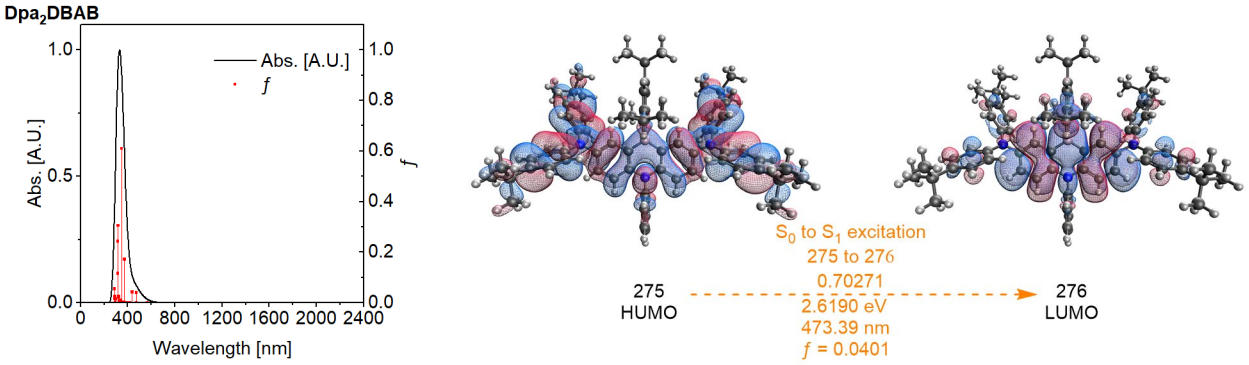

Figure S8. Simulated absorption spectra of **Dpa$_2$DBAB** with selected MOs relevant for calculated first allowed excited state.

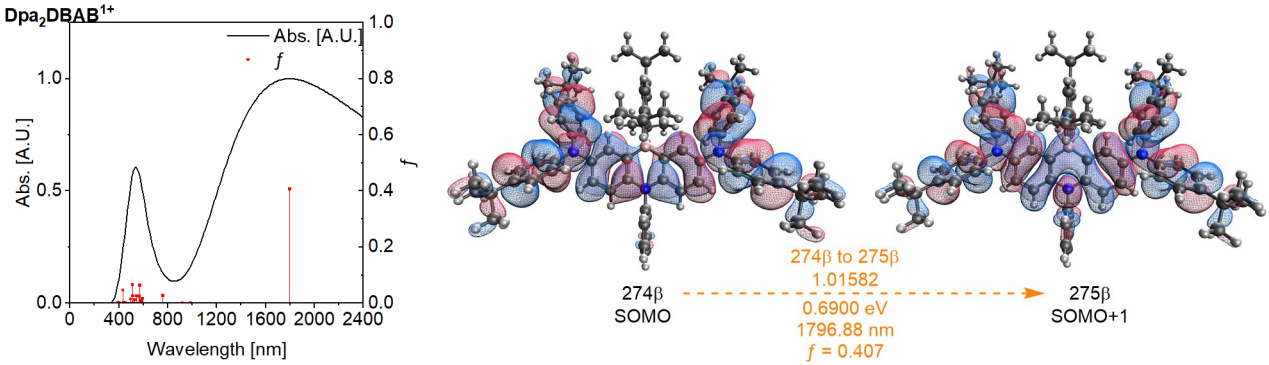

Figure S9. Simulated absorption spectra of **Dpa$_2$DBAB^{+}** with selected MOs relevant for calculated first allowed excited state

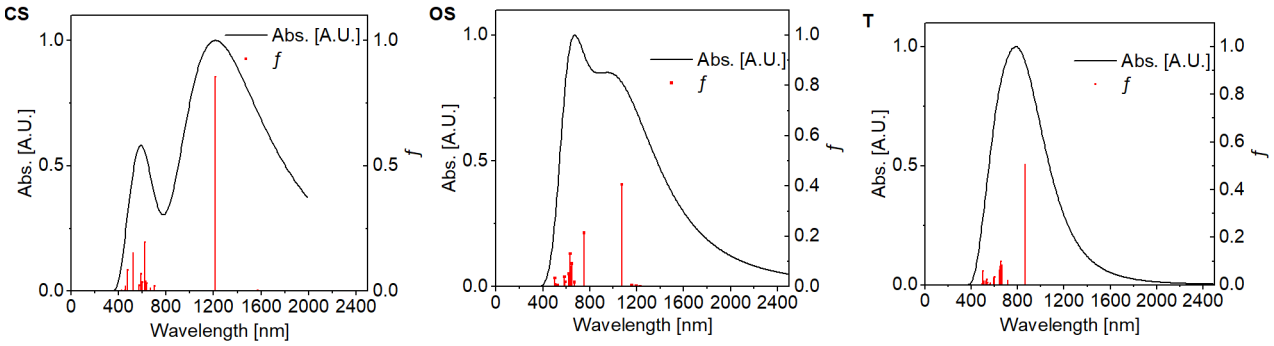

Figure S10. Simulated absorption spectra of **Dpa$_2$DBAB^{2+}** (right: **CS**, middle: **OS**, left: **T**)

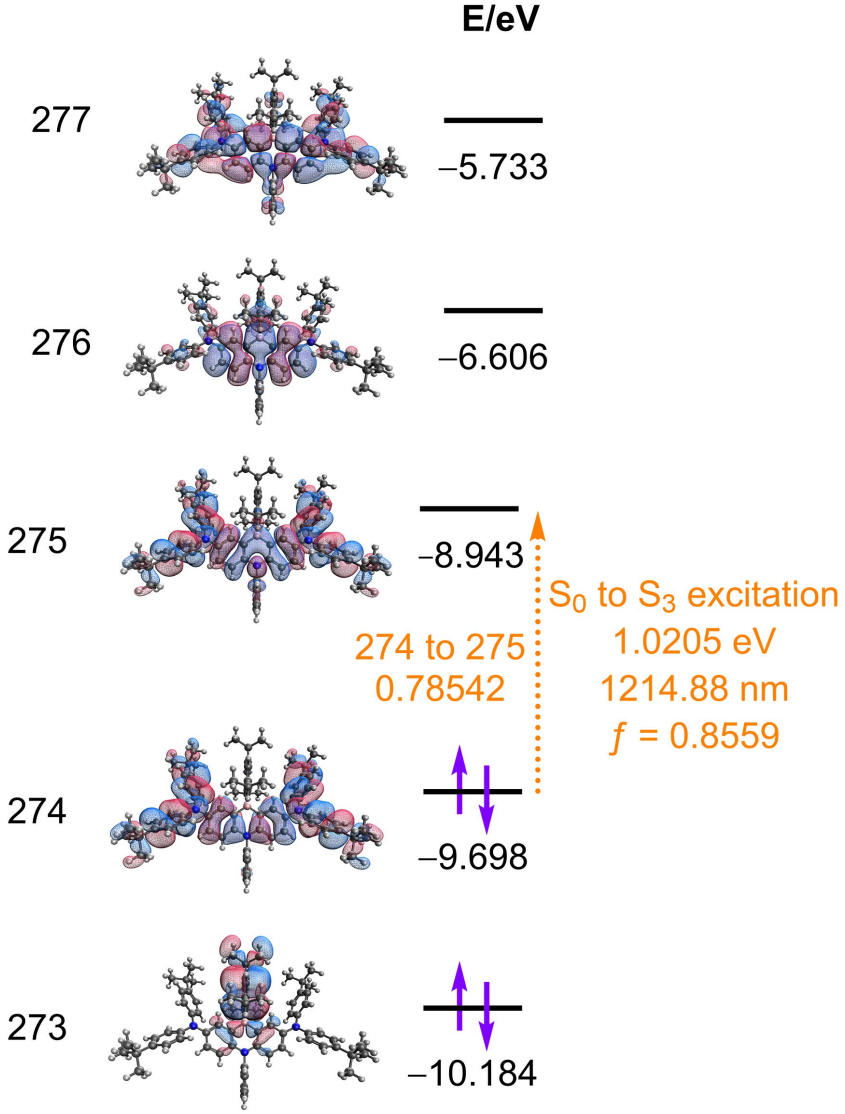

Figure S11. Selected MOs relevant for calculated first allowed excited state of **Dpa$_2$DBAB^{2+}** at **CS** state.

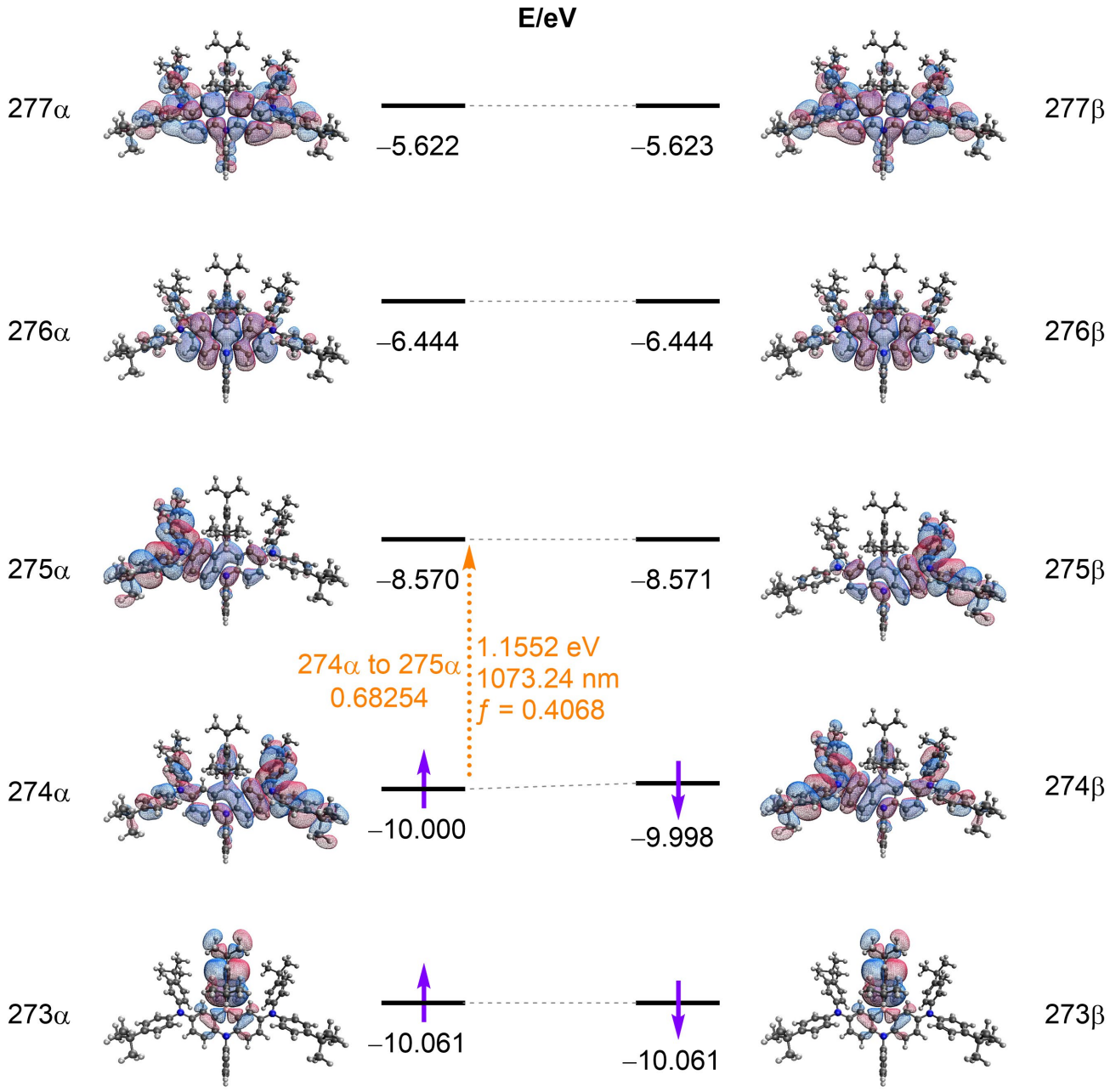

Figure S12. Selected MOs relevant for calculated first allowed excited state of **Dpa$_2$DBAB^{2+} (OS)**.

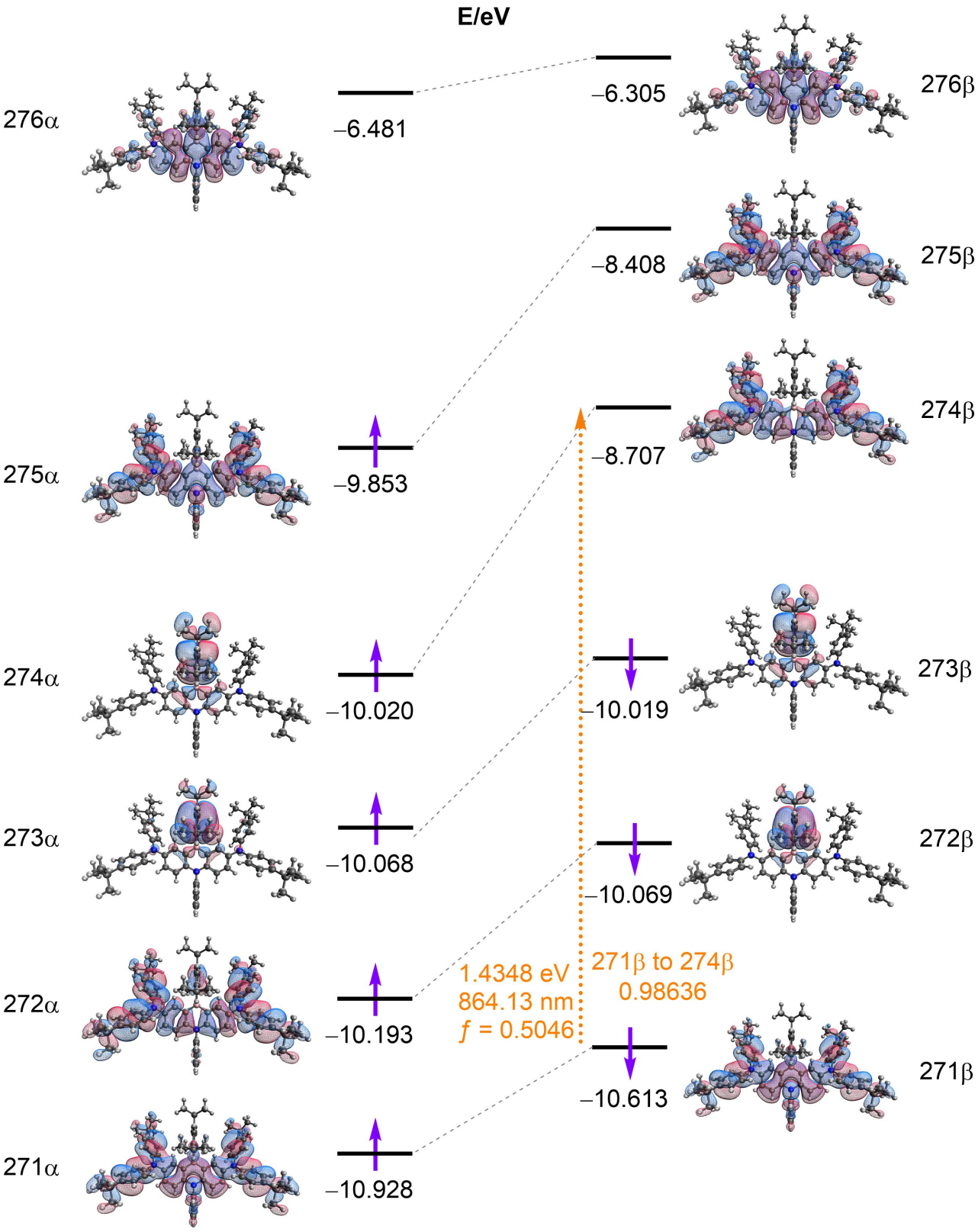

Figure S13. Selected MOs relevant for calculated first allowed excited state of **Dpa$_2$DBAB^{2+}** (**T**).

Supplemental details of NICS calculations

Based on the optimized ground state structure of **Dpa$_2$DBABA** and **Dpa$_2$DBAB^{2+}** at **CS**, **OS** and **T** sates, respectively, NICS(0) and NICS(1) values of the rings in dibenzo-1,4-azaborine moiety were calculated.[S12] The Bq atoms were added with py.Aroma (version 4.1.0).[S13] The XY Cartesian plane of geometries used to NICS(1)$_{zz}$ calculations were operated to parallel to the plane defined by the [1,4]-azaborine moiety with Multiwfn(version 3.8). [S14]

Table S10. Summary of methods used for TD-DFT calculations[a]

Compound		Method				Additional Conditions
Dpa$_2$DBAB[b]		HF	6-311+G(d)	Default Spin	B3LYP	-
Dpa$_2$DBAB^{2+}	scXRD[c]	HF	6-311G+(d)	Default Spin	B3LYP	-
	CS[b]	HF	6-311G+(d)	Default Spin	B3LYP	-
	OS[b]	UHF	6-311+G(d)	Unrestricted	B3LYP	guess=mix
	T[b]	UHF	6-311+G(d)	Unrestricted	B3LYP	-

[a] **CS** = closed-shell singlet, **OS** = open-shell singlet, **T** = triplet. [b] Calculated on geometries optimized at (U)B3LYP/6-311G(d) level. [c] Calculated on the scXRD geometry.

Table S11. Summary of calculated NICS(1)$_{zz}$ values of the rings in dibenzo-1,4-azaborine moiety

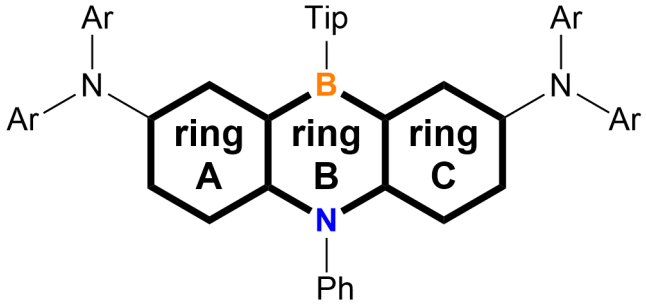

Compound		ring A		ring B		ring C	
		NICS (1)$_{zz}$ [ppm]	NICS (−1)$_{zz}$ [ppm]	NICS (1)$_{zz}$ [ppm]	NICS (−1)$_{zz}$ [ppm]	NICS (1)$_{zz}$ [ppm]	NICS (−1)$_{zz}$ [ppm]
Dpa$_2$DBAB		−26.9221	−26.4566	−6.2138	−5.7637	−26.9260	−26.4145
Dpa$_2$DBAB^{2+}	scXRD	−8.4502	−7.9671	+8.5886	+9.9581	−7.1072	−7.0676
	CS	−7.2121	−6.8684	+9.3248	+10.3244	−7.2831	−6.9468
	OS	−14.3435	−13.9333	−1.0983	−0.5336	−14.3516	−13.9483
	T	−16.7545	−16.2792	−2.9244	−2.4023	−16.7546	−16.2885

[a] **CS** = closed-shell singlet, **OS** = open-shell singlet, **T** = triplet. [b] Calculated on geometries optimized at (U)B3LYP/6-311G(d) level. [c] Calculated on the scXRD geometry.

Supplemental details of calculations on the Mulliken charge distribution

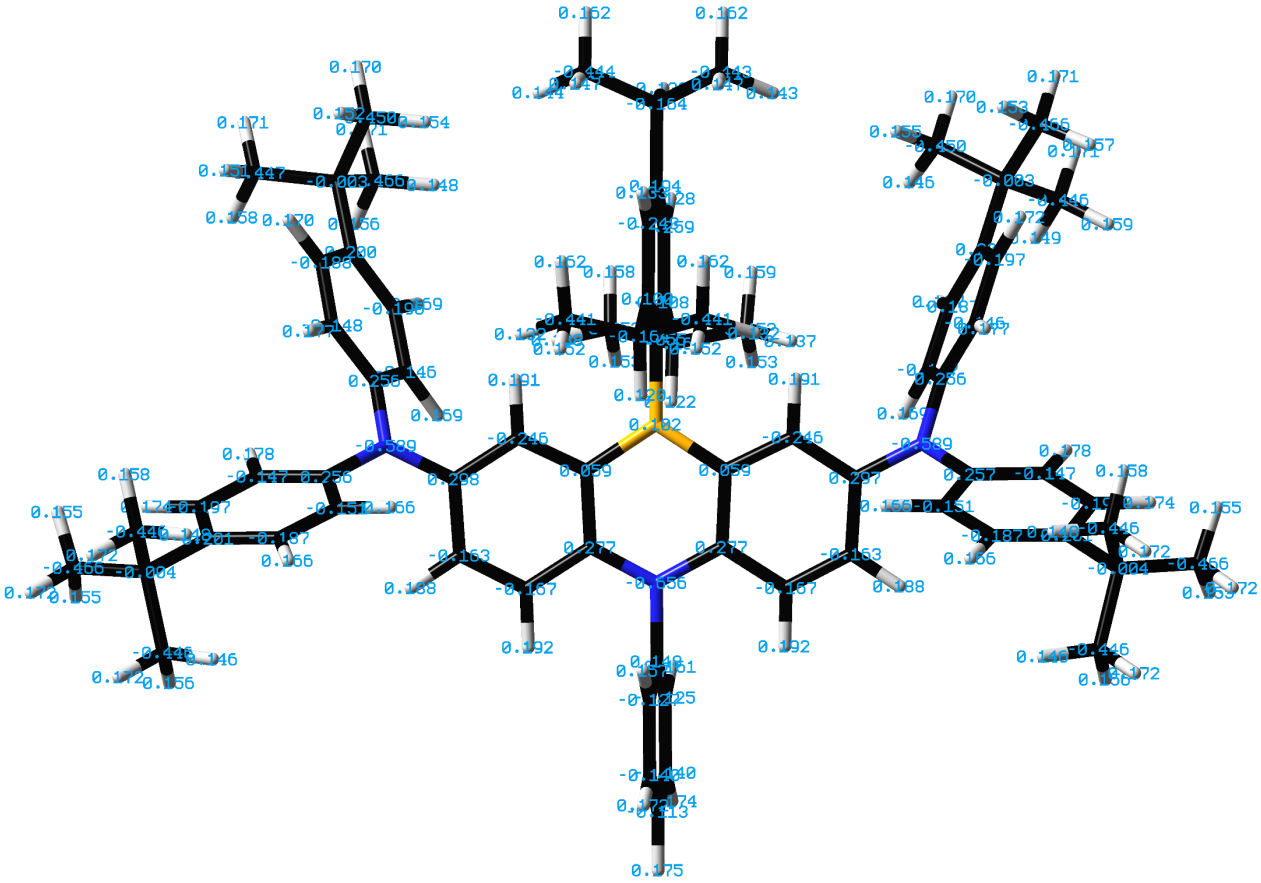

Figure S14. The Mulliken charge distribution of **Dpa$_2$DBAB^{2+}** at the **OS** state calculated at UB3LYP/6-311G(d) level.

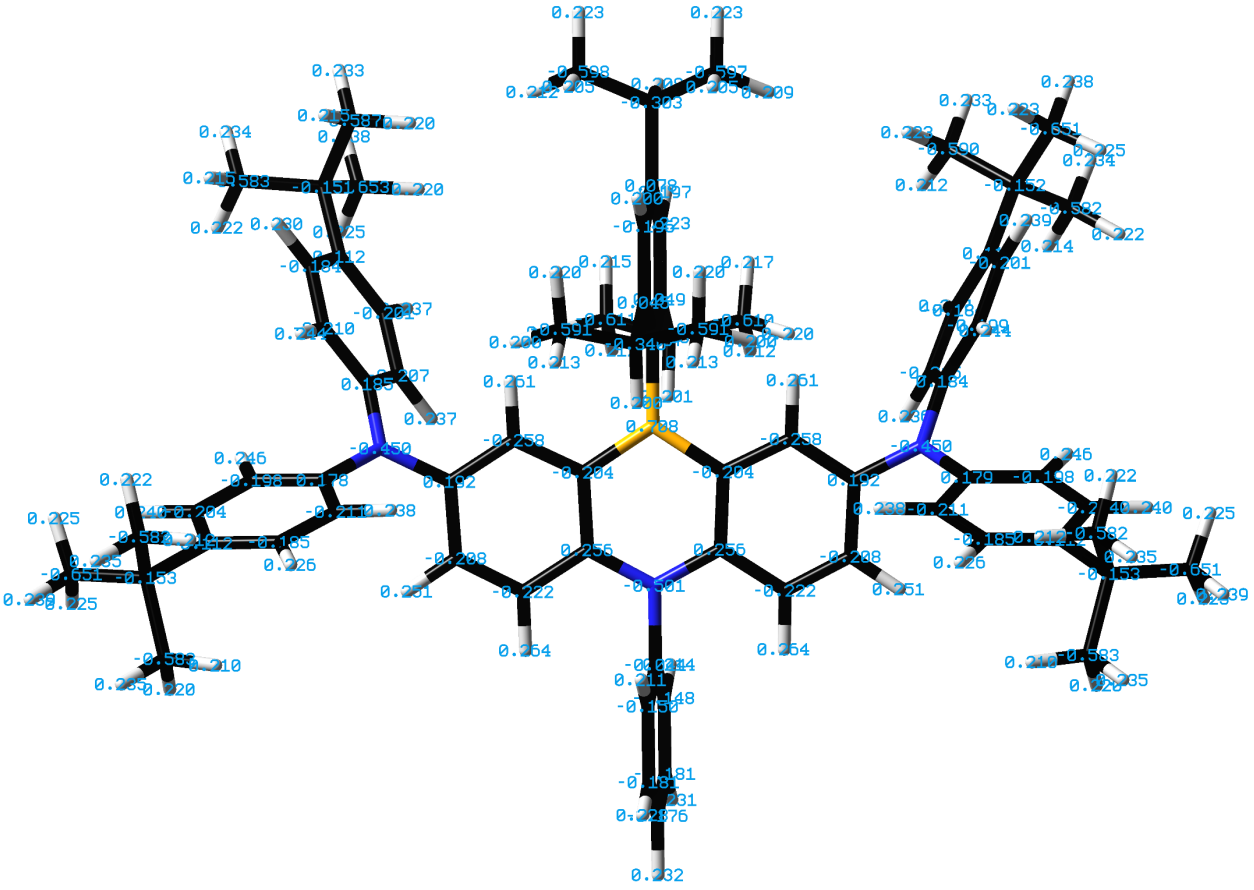

Figure S15. The Mulliken charge distribution of **Dpa$_2$DBAB^{2+}** at the **T** state calculated at UB3LYP/6-311G(d) level.

Supplemental details of calculations on spin density

Based on the optimized ground state structure of **Dpa$_2$DBAB^{2+}** at **OS** and **T** states, respectively, spin densities were calculated at UB3LYP/6-311G(d) level.

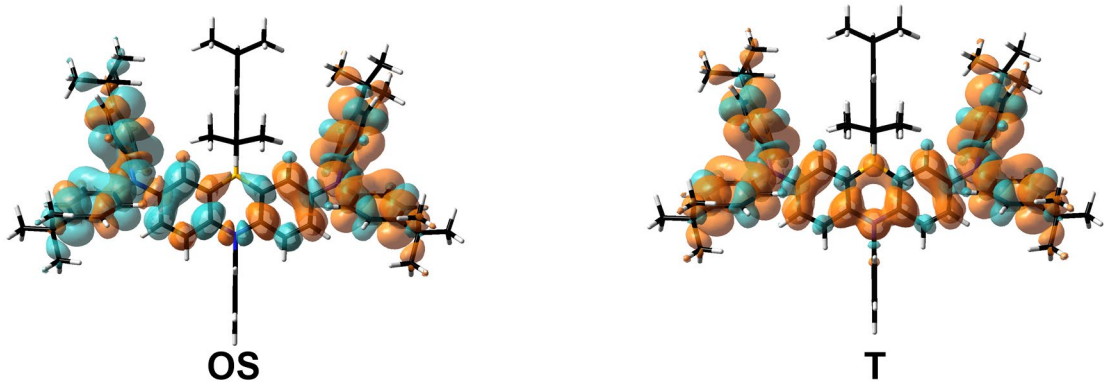

Figure S16. The spin density maps of **Dpa$_2$DBAB^{2+}** at the OS (right) and T (left) states calculated at UB3LYP/6-311G(d) level.

S7. References

[S1] T.-L. Wu, S.-H. Lo, Y.-C. Chang, M.-J. Huang, C.-H. Cheng, *ACS Appl. Mater. Interfaces* **2019**, *11*, 10768–10776.

[S2] S. Suzuki, K. Okada, *Organic Redox Systems*, (Ed.: T. Nishinaga), John Wiley & Sons, New Jersey, **2016**, Chapter 8, pp. 269–285.

[S3] O. V. Dolomanov, L. J. Bourhis, R. J. Gildea, J. A. K. Howard, H. Puschmann, *J. Appl. Cryst.* **2009**, 42, 339–341, (2009).

[S4] G. M. Sheldrick, *Acta Cryst.* **2015**, *71*, 3–8.

[S5] Deposition number 2387211 (for **[Dpa$_2$DBAB](SbF$_6$)$_2$**) contains the supplementary crystallographic data for this paper. This data are provided free of charge by the joint Cambridge Crystallographic Data Centre and Fachinformationszentrum Karlsruhe Access Structures service.

[S6] Gaussian 16, Revision C.02, M. J. Frisch, G. W. Trucks, H. B. Schlegel, G. E. Scuseria, M. A. Robb, J. R. Cheeseman, G. Scalmani, V. Barone, G. A. Petersson, H. Nakatsuji, X. Li, M. Caricato, A. V. Marenich, J. Bloino, B. G. Janesko, R. Gomperts, B. Mennucci, H. P. Hratchian, J. V. Ortiz, A. F. Izmaylov, J. L. Sonnenberg, D. Williams-Young, F. Ding, F. Lipparini, F. Egidi, J. Goings, B. Peng, A. Petrone, T. Henderson, D. Ranasinghe, V. G. Zakrzewski, J. Gao, N. Rega, G. Zheng, W. Liang, M. Hada, M. Ehara, K. Toyota, R. Fukuda, J. Hasegawa, M. Ishida, T. Nakajima, Y. Honda, O. Kitao, H. Nakai, T. Vreven, K. Throssell, J. A. Montgomery, Jr., J. E. Peralta, F. Ogliaro, M. J. Bearpark, J. J. Heyd, E. N. Brothers, K. N. Kudin, V. N. Staroverov, T. A. Keith, R. Kobayashi, J. Normand, K. Raghavachari, A. P. Rendell, J. C. Burant, S. S. Iyengar, J. Tomasi, M. Cossi, J. M. Millam, M. Klene, C. Adamo, R. Cammi, J. W. Ochterski, R. L. Martin, K. Morokuma, O. Farkas, J. B. Foresman, and D. J. Fox, Gaussian, Inc., Wallingford CT, 2019.

[S7] a) T. M. Krygowski, H. Szatylowicz, O. A. Stasyuk, J. Dominikowska, M. Palusiak, *Chem Rev.* **2014**, *114*, 6383–6422; b) J. Kruszewski, T.M. Krygowski, *Tetrahedron Lett.* **1972**, *13*, 3839; c) O. Bastiansen, M. Trætteberg, *Tetrahedron* **1962**, *17*, 147. d) Wilson, E. B., Jr.; Decius, J. C.; Cross, P. C. Molecular Vibrations, Dover, New York, **1955**, p. 174; e) *Physical Methods in Organic Chemistry*, Ed.: J. C. P. Schwarz, OLIVER & BOYD, Edinburgh & London, **1964**, p. 148. f) G. A. Jeffrey, J. R. Ruble, R. K. McMullan, J. A. Pople, *Proc. R. Soc. London* **1987**, *A414*, 47.

[S8] K. Yamaguchi, *Chem. Phys. Lett.* **1975**, *33*, 330–335.

[S9] a) K. Yamaguchi, Y. Takahara, T. Fueno, K. Nasu, Jpn. J. Appl. Phys. 1987, 26, L1362–L1364; b) K. Yamaguchi, F. Jensen, A. Dorigo, K. N. Houk, Chem. Phys. Lett. 1988, 149, 537–542.

[S10] C. F. Macrae, I. Sovago, S. J. Cottrell, P. T. A. Galek, P. McCabe, E. Pidcock, M. Platings, G. P. Shields, J. S. Stevens, M. Towler, P. A. Wood, *J. Appl. Cryst.* **2020**, *53*, 226–235.

[S11] Y. Su, X. Wang, Y. Li, Y. Song, Y. Sui, X. Wang, *Angew. Chem. Int. Ed.* **2015**, *54*, 1634–1637

[S12] a) Z. Chen, C. S. Wannere, C. Corminboeuf, R. Puchta, P. v. R. Schleyer, *Chem. Rev.* **2005**, *105*, 3842–3888; b) H. Fallah-Bagher-Shaidaei, C. S. Wannere, C. Corminboeuf, R. Puchta, P. v. R. Schleyer, *Org. Lett.* **2006**, *8*, 863–866. c) P. v. R. Schleyer, C. Maerker, A. Dransfeld, H. Jiao, N. J. R. v. E. Hommes, *J. Am. Chem. Soc.* **1996**, *118*, 6317–6318.

[S13] Z. Wang, *ChemRxiv preprint* **2024**, DOI: 10.26434/chemrxiv-2024-mjmj8.

[S14] a) T. Lu, F. Chen, *J. Comput. Chem.* **2012**, *33*, 580–592. b) T. Lu, *J. Chem. Phys.* **2024**, *161*, 082503.

S8. NMR Charts

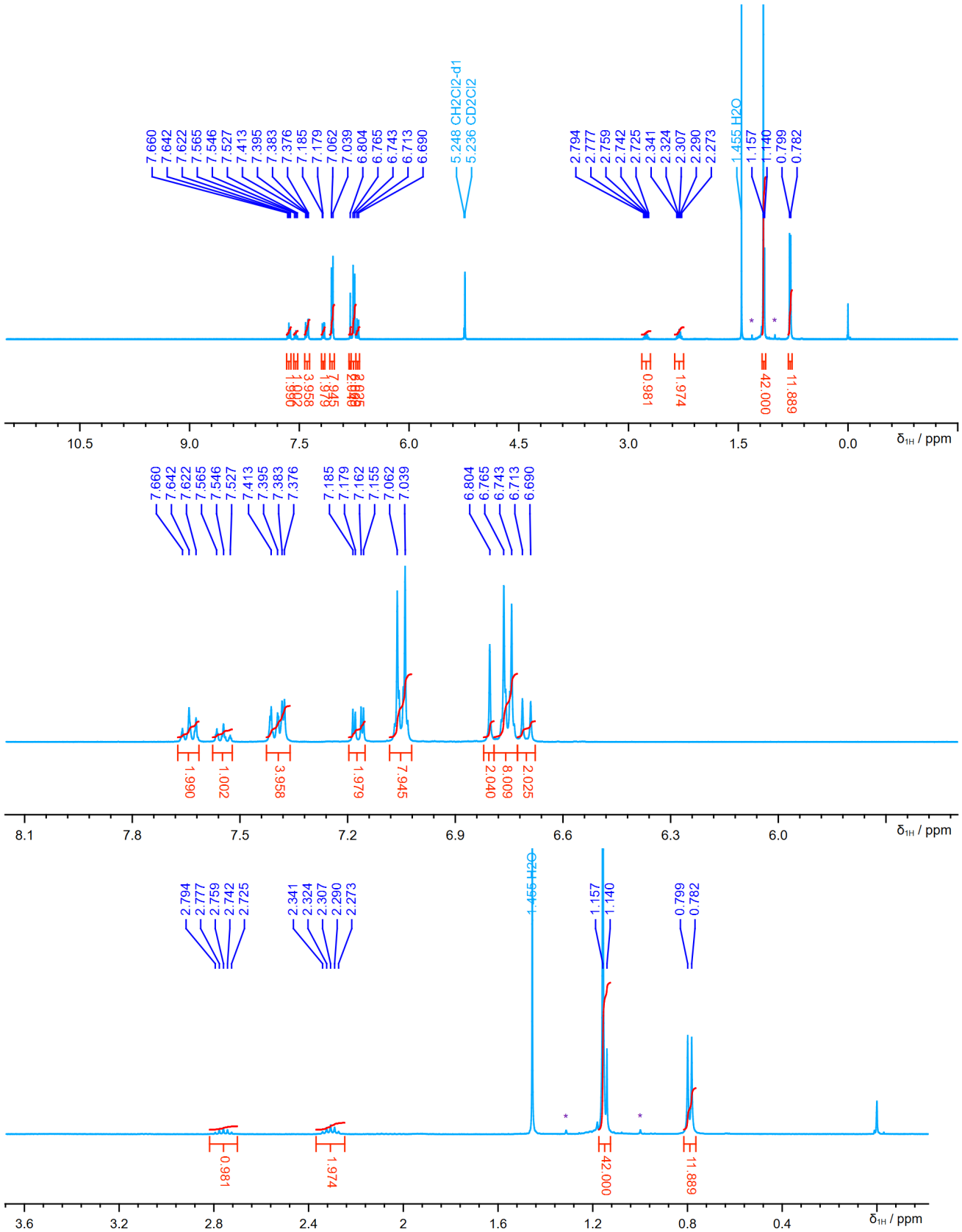

Figure S17. ^{1}H-NMR charts of **Dpa$_2$DBAB** in CD_2Cl_2 at 293 K(top: fullscale, middle: enlarged view of aromatic region, bottom: enlarged view of aliphatic region). *: side band.

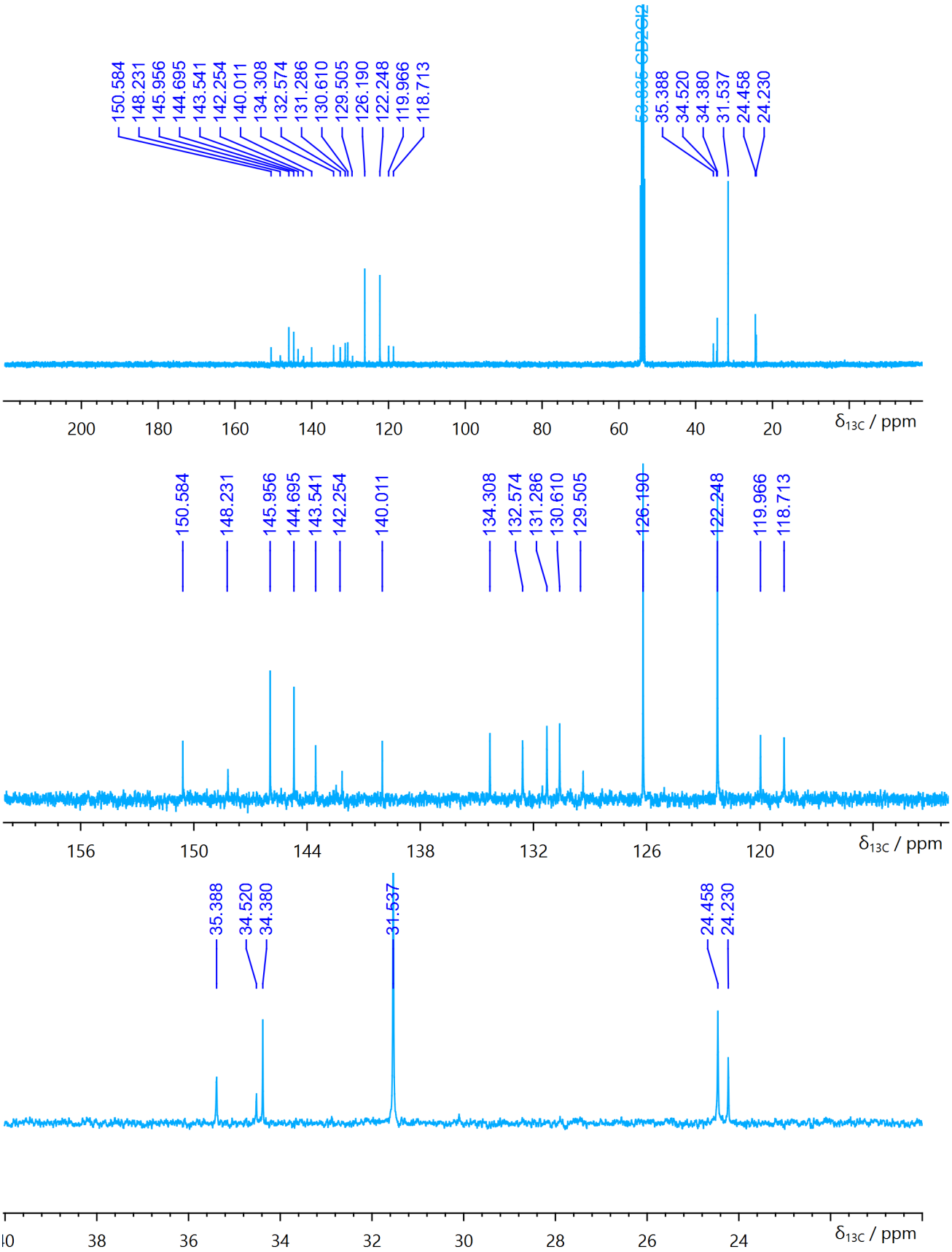

Figure S18. ^{13}C-NMR charts of **Dpa$_2$DBAB** in CD_2Cl_2 at 293 K (top: fullscale, middle: enlarged view of aromatic region, bottom: enlarged view of aliphatic region).

S9. HR-MS

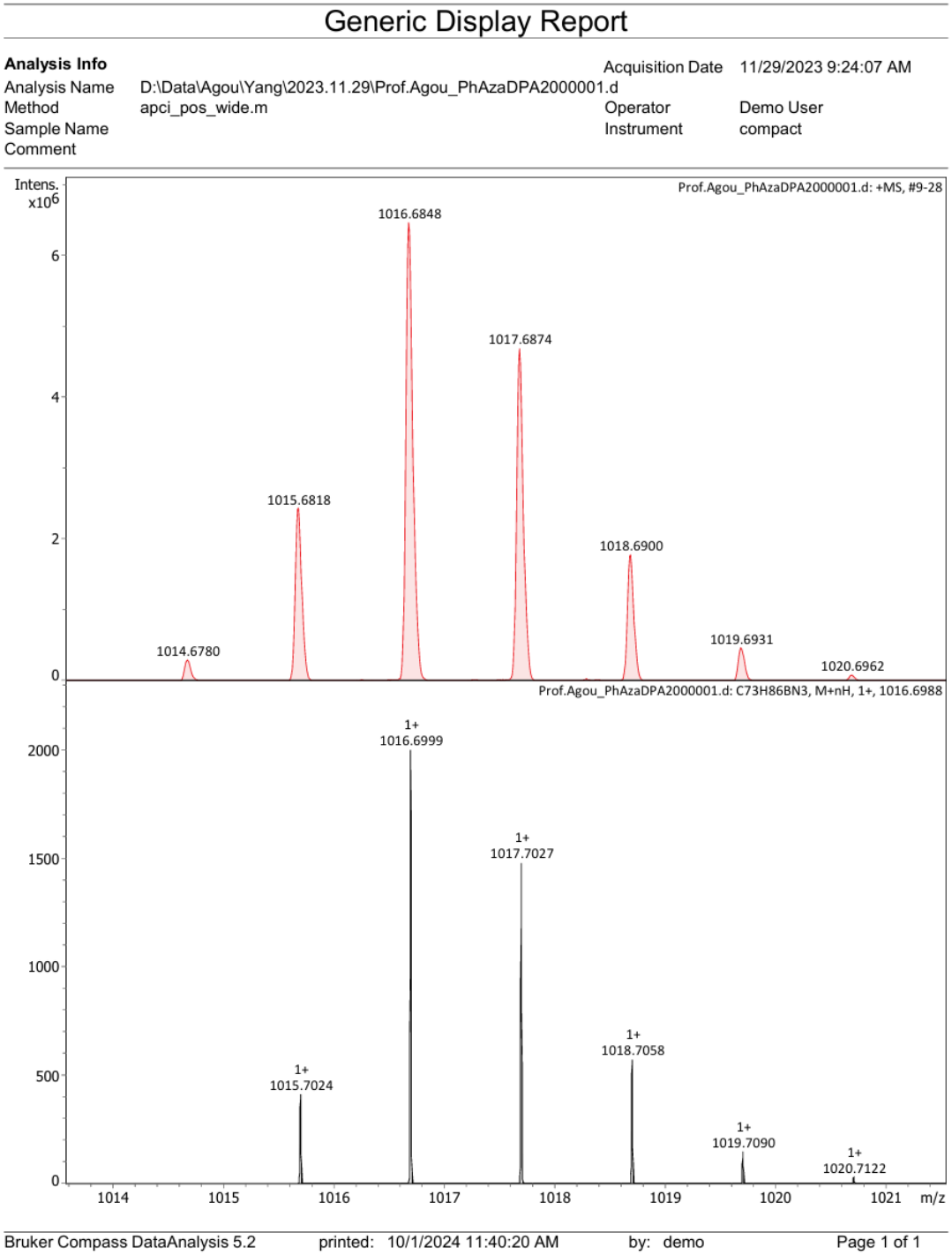

Figure S19. Isotopic patterns of the found parent ions **Dpa$_2$DBABA$^+$+nH** of recorded HR-MS of **Dpa$_2$DBABA** (APCI, Positive, in DCM).

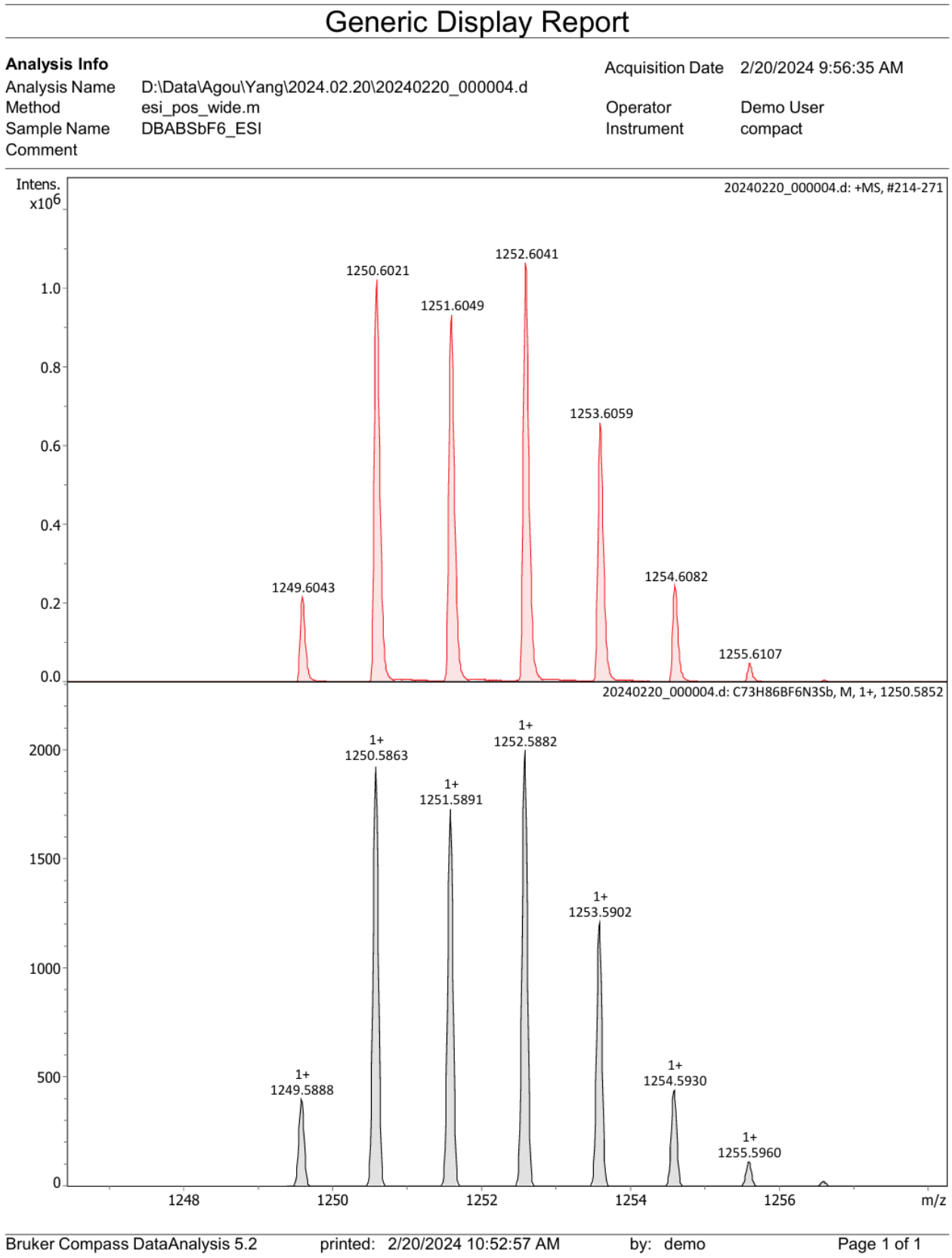

Figure S20. Isotopic patterns of the found parent ions **[Dpa$_2$DBABA](SbF$_6$)**$^+$ recorded in the HR-MS. of **[Dpa$_2$DBABA](SbF$_6$)$_2$** (ESI, Positive, in DCM).